

Effects of a first-order QCD phase transition on the enhancement of light nucleus yield ratio

He Liu,^{1,2,*} Kai-Jia Sun,^{3,4,†} and Peng-Cheng Chu^{1,2,‡}

¹Science School, Qingdao University of Technology, Qingdao 266520, China

²The Research Center of Theoretical Physics, Qingdao University of Technology, Qingdao 266033, China

³Key Laboratory of Nuclear Physics and Ion-beam Application (MOE),
Institute of Modern Physics, Fudan University, Shanghai 200433, China

⁴Shanghai Research Center for Theoretical Nuclear Physics,
NSFC and Fudan University, Shanghai 200438, China

(Dated: December 24, 2024)

Using an extended Nambu-Jona-Lasinio model to describe the baryon density fluctuations of quark matter along the isentropic trajectories corresponding to different s/ρ_B values extracted from Au+Au collisions at energies $\sqrt{s_{NN}} = 7.7 - 200$ GeV, we investigate the effects of the two-phase coexistence region during a first-order phase transition on the light nucleus yield ratio $N_t \times N_p/N_d^2$. The results indicate that the second-order scalar density moment y_2 , used to quantify density fluctuations, rapidly increases to form a peak when the isentropic trajectories pass through the coexistence region. We extract the yield ratios $N_t \times N_p/N_d^2$ at chemical freeze-out from the isentropic trajectories at different collision energies and found the significant enhancements at 19.6 GeV and 27 GeV. This is similar to the trends observed by the STAR experiment, suggesting that the enhancements in the yield ratios $N_t \times N_p/N_d^2$ observed in the STAR experiment should be attributed to the density fluctuations generated in the first-order phase transition region.

PACS numbers:

Introduction. Exploring the Quantum Chromodynamics (QCD) phase diagram of strongly interacting matter is one of the main goals of relativistic heavy-ion collisions [1, 2]. Lattice QCD (LQCD) simulations indicate that the transition between the quark-gluon plasma (QGP) and the hadronic matter is a smooth crossover at nearly zero baryon chemical potential (μ_B) [3–5]. Based on investigations from various effective models, such as the Nambu-Jona-Lasinio (NJL) model, as well as advanced functional methods including the Dyson-Schwinger equation (DSE) and the functional renormalization group (FRG) [6–15], the transition can be a first-order one at large μ_B region, resulting in a critical end point (CEP) on the first-order phase transition line. To search for the first-order phase transition and the potential CEP of QCD matter, experimental programs such as the Beam Energy Scan (BES-I and BES-II) have been carried out at the Relativistic Heavy-Ion Collider (RHIC) by varying the collision energy to cover a wide range of temperature T and μ_B in the QCD phase diagram [16, 17]. The STAR experiment has measured the energy dependence of observables that are sensitive to the CEP and/or first-order phase transition. Nonmonotonic energy dependencies were observed in these observables like net-proton fluctuations [18, 19], pion HBT radii [20, 21], baryon directed flow [22, 23], intermittency of charged hadrons [24], as well as light nucleus yield ratios [25].

Light nucleus production in heavy-ion collisions is an active area of research both experimentally [26–32] and theoretically [33–37]. The yield ratios $N_t \times N_p/N_d^2$ of tritons (N_t), deuterons (N_d), and protons (N_p) at $\sqrt{s_{NN}} = 7.7 - 200$ GeV have been measured by the STAR experiment at RHIC. In 0% – 10% most central Au + Au collisions at $\sqrt{s_{NN}} = 19.6$ and 27 GeV, the yield ratios $N_t \times N_p/N_d^2$ show significant enhancements relative to the coalescence baseline with a combined significance of 4.1σ [25]. Studies based on the coalescence models suggest that the fluctuations of neutron (baryon) density distributions and nucleon density-density correlations both lead to enhancements of the light nucleus yield ratios through the relation $N_t \times N_p/N_d^2 \approx \frac{1}{2\sqrt{3}}[1 + \Delta\rho_n + \frac{\lambda}{\sigma}G(\frac{\xi}{\sigma})]$, where $\Delta\rho_n$ is the average neutron density fluctuation, ξ is the correlation length, σ is related to the root-mean-square radius of deuteron or triton, λ is the parameter that varies smoothly with the temperature and the baryon chemical potential of the emission source, and function G denotes the contribution from the long-range correlation between neutrons and protons, which increases monotonically with ξ [35, 36]. When the system approaches CEP, although density fluctuation $\Delta\rho_n$ in a homogeneous system vanishes, the correlation length ξ becomes divergent. During the first-order phase transition where two phases coexist, however, the system could exhibit significant large density fluctuations [36, 38–40], despite the correlation lengths within each phase being much smaller than those near the critical point. Studies using hydrodynamic models [38, 39, 41, 42] and transport models [40, 43] have also shown that the minor initial inhomogeneities in heavy-ion collisions are amplified by spinodal instability when the produced matter crosses

*Electronic address: liuhe@qut.edu.cn

†Electronic address: kjsun@fudan.edu.cn

‡Electronic address: kyos@126.com

the first-order phase transition region in the QCD phase diagram. Therefore, the presence of a first-order phase transition and the proximity to the CEP can both enhance the yield ratio $N_t \times N_p/N_d^2$, provided these effects persist through the hadronic stage of the collision. This raises a question: Are the enhancements of light nucleus yield ratios observed by the STAR experiment at 19.6 and 27 GeV related to the first-order phase transition or critical region?

In the present study, we focus on investigating the effect of a first-order phase transition on baryon density fluctuations in QCD phase diagram based on an extended Nambu-Jona-Lasinio (NJL) model [44–46] including three eight-quark interactions [47–50]. The range of coexistence region during the first-order phase transition by varying the three eight-quark coupling constants can cover sufficiently the region that can be probed in realistic heavy-ion collisions. To quantify the baryon density fluctuations in full phase diagram theoretically, we consider using the second-order density moment y_2 as the physical quantity for our study, which is defined as $y_2 = \rho_B^2/\bar{\rho}_B^2 = [\int d\mathbf{x}\rho_B(\mathbf{x})][\int d\mathbf{x}\rho_B^3(\mathbf{x})]/[\int d\mathbf{x}\rho_B^2(\mathbf{x})]^2$, where $\rho_B(\mathbf{x})$ denotes the baryon density distribution in coordinate space. As shown in Refs. [35, 36, 51], the quantity $y_2 \approx 1 + \Delta\rho_B$ is directly related to the light nucleus yield ratios in heavy-ion collisions. The yield ratio $N_t \times N_p/N_d^2$ is approximately given by $y_2/(2\sqrt{3})$ when the correlation length is negligible. If the evolution of matter in the RHIC-BES can be approximated as an adiabatic expansion process, we can then calculate the density moment y_2 for isentropic trajectories corresponding to values of s/ρ_B within the ongoing RHIC-BES energy range and extract the yield ratios $N_t \times N_p/N_d^2$ at different collision energies. With this approach, we can reproduce the enhancements of yield ratios $N_t \times N_p/N_d^2$ due to the first-order phase transition in heavy ion collisions at $\sqrt{s_{NN}} = 19.6$ and 27 GeV.

Methods. In order to investigate the baryon density fluctuations along the experimental isentropic lines in a realistic 3-flavor NJL model which takes into account three eight-quark interactions [47–50]. The Lagrangian density can be given by

$$\begin{aligned} \mathcal{L}_{\text{NJL}}^{\text{SU}(3)} &= \bar{\psi}(i\partial - \hat{m})\psi + G_S \sum_{a=0}^8 [(\bar{\psi}\lambda^a\psi)^2 + (\bar{\psi}i\gamma_5\lambda^a\psi)^2] \\ &- K \{ \det[\bar{\psi}(1 + \gamma_5)\psi] + \det[\bar{\psi}(1 - \gamma_5)\psi] \} \\ &+ \mathcal{L}_1^{8q} + \mathcal{L}_2^{8q} + \mathcal{L}_{SV}^{8q}, \end{aligned} \quad (1)$$

where $\psi = (u, d, s)^T$ represents the quark fields with three flavors, $\hat{m} = \text{diag}(m_u, m_d, m_s)$ is the current quark mass matrix, and λ^a are the flavor SU(3) Gell-Mann matrices with $\lambda_0 = \sqrt{2/3}I$. G_S is the scalar coupling constant, and the K term represents the six-point Kobayashi-Maskawa-t' Hooft (KMT) interaction that breaks the axial symmetry $U(1)_A$ [52]. \mathcal{L}_1^{8q} and \mathcal{L}_2^{8q} are

TABLE I: Parameters in the extended NJL model

$m_{u,d}(\text{MeV})$	$m_s(\text{MeV})$	$\Lambda(\text{MeV})$	$G_S\Lambda^2$
5.5	183.468	637.720	3.02
$K\Lambda^5$	$G_1(\text{MeV}^{-8})$	$G_2(\text{MeV}^{-8})$	$G_{SV}\Lambda^8$
9.496	2.193×10^{-21}	-1.890×10^{-22}	-3500.00

the eight-quark interaction terms described by [47, 48]

$$\mathcal{L}_1^{8q} = \frac{G_1}{2} \{ [\bar{\psi}_i(1 + \gamma_5)\psi_j][\bar{\psi}_j(1 - \gamma_5)\psi_i] \}^2, \quad (2)$$

and

$$\begin{aligned} \mathcal{L}_2^{8q} &= G_2 \{ [\bar{\psi}_i(1 + \gamma_5)\psi_j][\bar{\psi}_j(1 - \gamma_5)\psi_k] \\ &\times [\bar{\psi}_k(1 + \gamma_5)\psi_l][\bar{\psi}_l(1 - \gamma_5)\psi_i] \}. \end{aligned} \quad (3)$$

These two the eight-quark interaction terms with coupling constants G_1 and G_2 in the Lagrangian could solve the problem of unstable vacuum in NJL Model. The main effect of the eight-quark interaction terms is to shift the crossover region to $T_0 \approx 162$ MeV at vanishing baryon chemical potential, thus bringing them closer to lattice QCD results and the experimental freeze-out line. In above Eq.(1), the term \mathcal{L}_{SV}^{8q} is an eight-quark scalar-vector interaction given by [49, 50]

$$\begin{aligned} \mathcal{L}_{SV}^{8q} &= G_{SV} \{ \sum_{a=1}^3 [(\bar{\psi}\lambda^a\psi)^2 + (\bar{\psi}i\gamma_5\lambda^a\psi)^2] \} \\ &\times \{ \sum_{a=1}^3 [(\bar{\psi}\gamma^\mu\lambda^a\psi)^2 + (\bar{\psi}\gamma_5\gamma^\mu\lambda^a\psi)^2] \}. \end{aligned} \quad (4)$$

Although the eight-quark scalar-vector coupled interaction has no effects on the QCD vacuum properties and on the phase transition boundary in the QCD phase diagram, the strength of scalar-vector interactions G_{SV} can change the critical temperature and baryon chemical potential. As shown in Ref. [43, 49, 50], with a negative G_{SV} the critical point moves to higher temperature and lower baryon chemical potential (or baryon density). Therefore, the range of spinodal region by varying the three eight-quark coupling constants (G_1 , G_2 , and G_{SV}) can cover sufficiently the region that can be probed in realistic heavy-ion collisions. In this work, the different parameters [47, 48] in the extended NJL model are given in Table I.

In the mean-field approximation, the thermodynamic potential from the finite-temperature field theory can be expressed as

$$\begin{aligned} \Omega_{\text{NJL}} &= -2N_c \sum_i \int \frac{d^3p}{(2\pi)^3} [E_i + T \ln(1 + e^{-\beta(E_i - \tilde{\mu}_i)}) \\ &+ T \ln(1 + e^{-\beta(E_i + \tilde{\mu}_i)})] + G_S(\sigma_u^2 + \sigma_d^2 + \sigma_s^2) \\ &- 4K\sigma_u\sigma_d\sigma_s + \frac{3}{2}G_1(\sum_i \sigma_i^2)^2 + 3G_2 \sum_i \sigma_i^4 \\ &+ 3G_{SV}(\sigma_u + \sigma_d)^2(\rho_u + \rho_d)^2, \end{aligned} \quad (5)$$

where the factor $2N_c = 6$ represents the spin and color degeneracy of the quark, $\beta = 1/T$ is the inverse of the temperature. It is worth noting that the first integral term, which corresponds to the vacuum contribution, exhibits ultraviolet divergence. This necessitates the introduction of a cutoff parameter Λ (as detailed in Table I) to regularize the three-momentum integration. In the above, $E_i = \sqrt{M_i^2 + p^2}$ is the single-quark energy for quark flavor i , where M_i is the constituent mass given by the gap equations

$$\begin{aligned}
 M_u &= m_u - 2G_S\sigma_u + 2K\sigma_d\sigma_s - 2G_1\sigma_u\left(\sum_i \sigma_i^2\right) - 4G_2\sigma_u^3 \\
 &\quad - 2G_{SV}(\rho_u + \rho_d)^2(\sigma_u + \sigma_d), \\
 M_d &= m_d - 2G_S\sigma_d + 2K\sigma_s\sigma_u - 2G_1\sigma_d\left(\sum_i \sigma_i^2\right) - 4G_2\sigma_d^3 \\
 &\quad - 2G_{SV}(\rho_u + \rho_d)^2(\sigma_u + \sigma_d), \\
 M_s &= m_s - 2G_S\sigma_s + 2K\sigma_u\sigma_d - 2G_1\sigma_s\left(\sum_i \sigma_i^2\right) - 4G_2\sigma_s^3.
 \end{aligned}
 \tag{6}$$

The effective chemical potential $\tilde{\mu}_i$ can be expressed as

$$\begin{aligned}
 \tilde{\mu}_u &= \mu_u + 2G_{SV}(\rho_u + \rho_d)(\sigma_u + \sigma_d)^2, \\
 \tilde{\mu}_d &= \mu_d + 2G_{SV}(\rho_u + \rho_d)(\sigma_u + \sigma_d)^2, \\
 \tilde{\mu}_s &= \mu_s,
 \end{aligned}
 \tag{7}$$

where μ_i denotes the i th quark chemical potential. In our calculation, we set $\mu_u = \mu_d = \mu_s = \mu_B/3$, where μ_B is the baryon chemical potential. $\sigma_i = \langle \bar{\psi}_i \psi_i \rangle$ stands for quark condensate, which serves as the order parameter for the chiral phase transition. From the thermodynamic potential given by Eq. (5), the physical values for the condensates σ_i can be calculated considering the following equation $\frac{\partial \Omega_{\text{NJL}}}{\partial \sigma_i} = 0$. The pressure, number density, and entropy density can be derived using the thermodynamic relations in the grand canonical ensemble as $P = -\Omega_{\text{NJL}}$, $\rho_i = -\frac{\partial \Omega_{\text{NJL}}}{\partial \mu_i}$, and $s = -\frac{\partial \Omega_{\text{NJL}}}{\partial T}$.

Density fluctuations and enhancements of light nucleus yield ratios. We first display the phase diagram from the NJL model for quark matter in $T - \rho_B$ plane in Fig. 1. The gray dash-dotted line depicts the boundary of the two-phase coexistence region, where the two phases within this region satisfy the thermodynamic equilibrium conditions of equal pressure, temperature, and chemical potential. For the liquid-gas-like phase transition, e.g., the NJL model, the chemical potential in the liquid-gas mixed phase can be regarded as that of the first-order chiral phase transition boundary in $T - \mu_B$ plane. The mechanical (spinodal) instability regions with $(\partial P / \partial \rho_B)_T < 0$ are also displayed in the shaded region. The black dashed line and dot are respectively for the chiral crossover and CEP that connect the chiral crossover and coexistence region. It can be observed that due to the effect of the coupling constants G_1 and G_2 , the crossover temperature at vanishing baryon density is

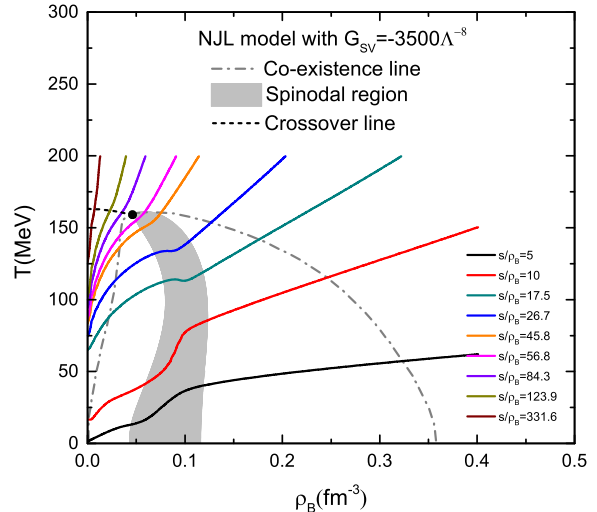


FIG. 1: Phase diagram from an extended NJL model for quark matter in $T - \rho_B$ plane. The gray dash-dotted line represents the boundary of the two-phase coexistence region, and the shaded region is the mechanical (spinodal) instability regions with $(\partial P / \partial \rho_B)_T < 0$. The black dashed line and dot are respectively for the chiral crossover and CEP that connect the chiral crossover and coexistence region. The different color solid lines represent isentropic trajectories of the s/ρ_B values listed in Table 2.

approximately 162 MeV, which is consistent with the predictions from Lattice QCD calculations and experimental results [53–56]. More importantly, with the vector-scalar interaction coupling constant $G_{SV} = -3500\Lambda^{-8}$, the CEP temperature ($T_c > 150$ MeV) is significantly increased compared to the default NJL model, which results in a larger coexistence region, allowing the evolution trajectory of higher-energy heavy-ion collisions to pass through the coexistence region. In heavy-ion collisions, the produced system undergoes an approximately isentropic expansion driven by pressure gradients along trajectories of constant entropy per baryon ($s/\rho_B = \text{const}$), when dissipative effects such as viscosity, heat conduction, and charge diffusion are neglected. In order to provide phenomenological analysis for the BES program at RHIC, we need to estimate the entropy per baryon and the initial entropy density of the system at various Au+Au collision energies from 7.7 to 200 GeV. The initial entropy density s_0 could be estimated by assuming that its value is proportional to the measured rapidity density of charged particles $dN_{ch}/d\eta$ [57]. For Au+Au collisions at $\sqrt{s_{NN}} = 200$ GeV the value of s_0 is about 84 fm^{-3} [58], and the initial entropy density at lower collision energies is obtained rescaling the estimate at $\sqrt{s_{NN}} = 200$ GeV according to dN_{ch}/dy [55, 56]. If using s_0 as the initial condition in hydrodynamic calculations can successfully reproduce the soft hadron distribu-

TABLE II: Estimate of the initial entropy density and of the entropy per baryon in Au+Au collisions at different collision energies. The kinetic and chemical freeze-out temperatures are obtained in Refs. [55, 56].

$\sqrt{s_{NN}}$ (GeV)	s_0 (fm $^{-3}$)	s/ρ_B	T_{kin}^{fo}	T_{ch}^{fo}
7.7	29.6	17.5	116	143
11.5	35.3	26.7	118	151
19.6	43.0	45.8	113	158
27.0	45.8	56.8	117	160
39.0	47.6	84.3	117	160
62.4	60.2	123.9	99	161
200	84.0	331.6	89	162

tions, then the s/ρ_B ratios at different collision energies can be extracted from the yields of identified hadrons ($\pi^\pm, K^\pm, p/\bar{p}$). As shown in Ref. [57], the results for s_0 and s/ρ_B at $\sqrt{s_{NN}} = 7.7 - 200$ GeV are collected in Table 2, where we also display the values of the kinetic and chemical freeze-out temperatures obtained in Ref. [55, 56]. In Fig. 1, we depict the isentropic trajectories of the s/ρ_B values listed in Table 2 using solid lines of different colors. In addition, the isentropic lines with $s/\rho_B = 5, 10$ are shown for comparison. It can be seen that, with the coupling constant set in our model, the trajectories corresponding to $s/\rho_B < 56.8$ for collision energies below 39 GeV pass through the coexistence region of the phase diagram, which could lead to enhanced density fluctuations in the systems produced at these collision energies.

The size of the coexistence region in the QCD phase diagram affects the observation of first-order phase transitions in heavy-ion collisions. This is because the rapid development of baryon density fluctuations as the produced quark matter evolves through the coexistence region of the QCD phase diagram leads to clustering [38, 59], making it easier for light nuclei to form [59]. As shown in Refs. [35, 36] based on the nucleon coalescence model, the yield ratio $N_t \times N_p/N_d^2$ is approximately given by the second order scaled density moment $y_2/(2\sqrt{3})$, if the density-density correlation length is zero. In two-phase coexistence region, the densities of the dense and dilute phases are determined by the Maxwell's construction, and thus the second order scaled density moment can be given by $y_2 = (\rho_1 \lambda_1 + \rho_2 \lambda_2)(\rho_1^3 \lambda_1 + \rho_2^3 \lambda_2)/(\rho_1^2 \lambda_1 + \rho_2^2 \lambda_2)^2$, where ρ_i and λ_i for $i = 1, 2$ are respectively the baryon densities and volume fractions of the dense and dilute phases. In the upper panel of Fig. 2, we present the contour map of y_2 in the full phase diagram based on the extended NJL model with the coupling constant $G_{SV} = -3500\Lambda^{-8}$. It can be seen that y_2 clearly delineates the extent of the coexistence region. In the non-coexistence (white) region, y_2 takes the constant value $y_2 = 1$ due to the absence of density fluctuations, whereas y_2 is significantly enhanced in the coexistence (colored) region, especially on the left side of the coexistence re-

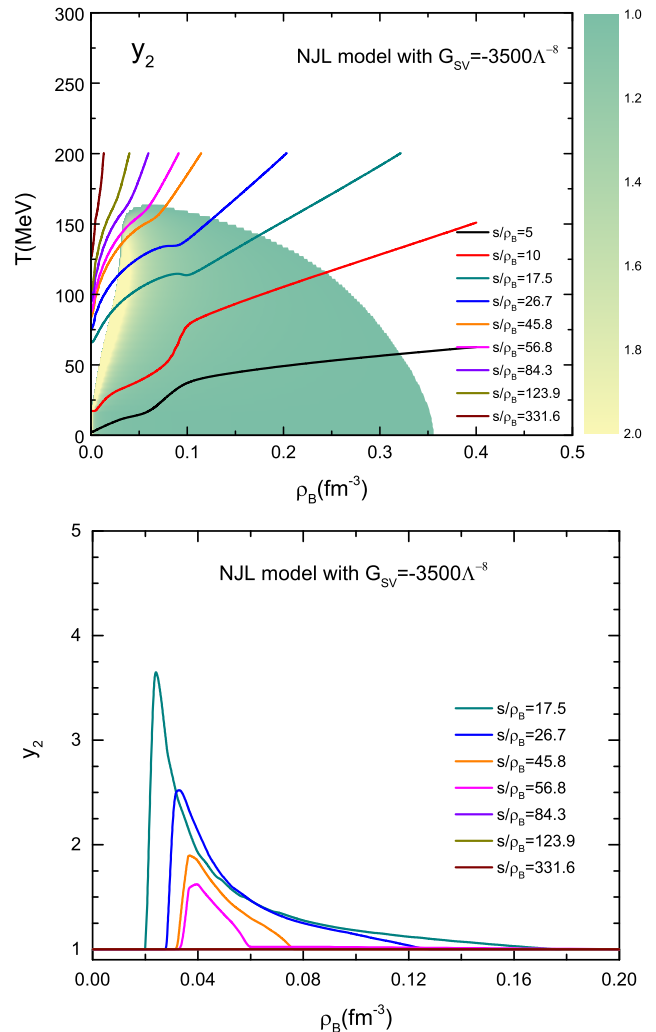


FIG. 2: Upper panel: the contour map of y_2 in the full phase diagram based on the extended NJL model with the coupling constant $G_{SV} = -3500\Lambda^{-8}$. The different color solid lines represent isentropic trajectories of the s/ρ_B values for different collision energies listed in Table 2. Besides, the isentropics lines with $s/\rho_B = 5, 10$ are shown for comparison. Lower panel: y_2 as functions of ρ_B along the isentropic trajectories of the s/ρ_B values for different collision energies listed in Table 2.

gion. To better describe the changes in density fluctuations at different energies during the evolution of heavy-ion collisions, the results for y_2 as functions of ρ_B along the isentropic trajectories of the s/ρ_B values are shown in the lower panel of Fig. 2 by the different colored solid lines. It can be seen that as the isentropic trajectories pass through the coexistence region, y_2 rapidly increases to form a peak and then gradually decreases back to 1. We can also observe that the peak value of

y_2 increases as the entropy per baryon (collision energy) decreases. The increase in density fluctuations leads to enhanced clustering, which facilitates the production of light nuclei. Therefore, the yield of light nuclei increases as the collision energy decreases. The experiments that the energy dependence of N_d/N_p and N_t/N_p ratios in the midrapidity of central heavy-ion collisions from the FOPI [60], E864 [27], PHENIX [61], and ALICE [29] also confirm this point. The results indicate both N_d/N_p and N_t/N_p ratios increase monotonically with decreasing collision energy. In addition, the coalescence model, which predicts light nuclei production at midrapidity based on baryon density (ρ_B) via the relationship $N_A/N_p \propto \rho_B^{A-1}$, can also describe similar energy dependence trends [62].

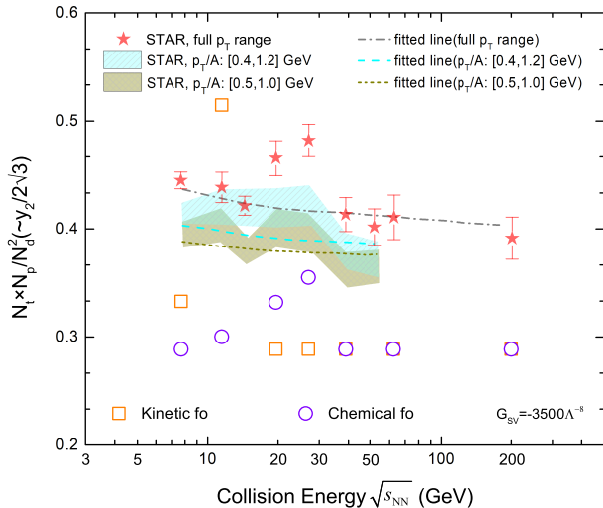


FIG. 3: Collision energy dependence of the yield ratio $N_t \times N_p / N_d^2$, where the yield ratio is approximated by $y_2 / (2\sqrt{3})$. The violet open circles correspond to the results at chemical freeze-out during the isentropic process at different energies, while the orange open squares represent the results at kinetic freeze-out. The results from 0%-10% central Au + Au collisions at RHIC are also shown for comparison. Red solid stars with error bars are the final results with extrapolation to the full p_T range and the dash-dotted fitted lines are the coalescence baselines from the coalescence-inspired fit. The colored bands and dashed fitted lines denote p_T acceptance dependence, for which the statistical and systematic uncertainties are added in quadrature.

As mentioned in *Introduction*, the yield ratio $N_t \times N_p / N_d^2$ is predicted to be sensitive to the local baryon density fluctuations and critical correlation lengths, which could be used to probe the first-order phase transition and/or CEP in heavy-ion collisions. To determine whether the enhancements of light nucleus yield ratios observed by the STAR experiment at 19.6 and 27 GeV is related to a first-order phase transition, we present in Fig. 3 the collision energy dependence of the yield ratio $N_t \times N_p / N_d^2$, where the yield ratio is approximated by

$y_2 / (2\sqrt{3})$, neglecting the effect of the correlation length. The violet open circles correspond to the results at chemical freeze-out during the isentropic process at different energies, while the orange open squares represent the results at kinetic freeze-out. The temperatures for chemical and kinetic freeze-out are obtained from Ref. [55, 56], as shown in Table 2. The results from 0%-10% central Au + Au collisions at RHIC are also shown for comparison. Red solid stars with error bars are the final results with extrapolation to the full p_T range and the dash-dotted fitted lines are the coalescence baselines from the coalescence-inspired fit. The colored bands and dashed fitted lines denote p_T acceptance dependence, for which the statistical and systematic uncertainties are added in quadrature. Our results indicate that the yield ratios $N_t \times N_p / N_d^2$ at kinetic freeze-out show the significant enhancements at collision energies 7.7 and 11.2 GeV. Encouragingly, the enhancements of yield ratios at chemical freeze-out occurs at 19.6 and 27 GeV, which is similar to the trends observed by the STAR experimental. This suggests that the enhancements in the yield ratios $N_t \times N_p / N_d^2$ observed in the STAR experiment can be attributed to the density fluctuations generated in the first-order phase transition region. However, we also note that the overall ratios obtained from our calculations are lower than the experimental results and the baseline provided by the coalescence model, which is due to the neglect of the density-density correlation length. Recently, the non-monotonic dependence of net-proton fluctuations, which are sensitive to the correlation length, on collision energy has indeed been observed in the preliminary data from the STAR Collaboration, particularly the dip structure around 19.6 GeV. Therefore, we cannot rule out the possibility that the critical region could also lead to the enhancements in the yield ratios in the range of 19.6 to 27 GeV. In future work, we will further explore the effects of the correlation length in the critical region on the light nucleus yields ratios, and integrate the extended NJL model and its parameters into transport models to investigate the structure of the QCD phase diagram.

Summary and outlook. Based on an extended Nambu-Jona-Lasinio (NJL) model with three eight-quark interactions, we investigate the effects of the two-phase coexistence region during a first-order phase transition on light nuclei production in QCD phase diagram. The range of coexistence region by varying the three eight-quark coupling constants (G_1 , G_2 , and G_{SV}) can cover sufficiently the region that can be probed in realistic heavy-ion collisions. Considering the evolution of matter in heavy-ion collisions as an isentropic process, we use the second-order scalar density moment y_2 approximation to calculate the baryon density fluctuations along the isentropic trajectories corresponding to different s/ρ_B values extracted from Au+Au collisions at energies ranging from 7.7 to 200 GeV at RHIC. Results indicate that y_2 rapidly increases to form a peak when the isentropic trajectories pass through the coexistence region due to the density fluctuations in the first-order phase transition region.

We extracted the yields ratios $N_t \times N_p/N_d^2$ at chemical freeze-out from the isentropic trajectories at different collision energies and found the significant enhancements at 19.6 GeV and 27 GeV, which is similar to the trends observed by the STAR experimental. This suggests that the enhancements in the yield ratios $N_t \times N_p/N_d^2$ observed in the STAR experiment can be attributed to the density fluctuations generated in the first-order phase transition region. Due to the lack of studies on the correlation length in the critical region, we cannot rule out the possibility that the critical region could also lead to

the enhancements in the yield ratios in the range of 19.6 to 27 GeV. Further studies from transport modeling of heavy-ion collisions will be conducted to confirm if the enhancements are due to large density fluctuations during a first-order phase transition.

This work is supported by the National Natural Science Foundation of China under Grants No. 12205158, and No. 11975132, as well as the Shandong Provincial Natural Science Foundation, China Grants No. ZR2021QA037, No. ZR2022JQ04, and No. ZR2019YQ01.

-
- [1] X. Luo and N. Xu, Nucl. Sci. Tech. **28**, 112 (2017).
- [2] A. Bzdak, S. Esumi, V. Koch, J. Liao, M. Stephanov, and N. Xu, Phys. Rept. **853**, 1 (2020).
- [3] Y. Aoki, G. Endrődi, Z. Fodor, S.D. Katz, and K.K. Szabó, Nature (London) **443**, 675 (2006).
- [4] S. Gupta, X.F. Luo, B. Mohanty, H.G. Ritter, and N. Xu, Science **332**, 1525 (2011).
- [5] S. Borsányi, Z. Fodor, C. Hoelbling, S.D. Katz, S. Krieg, and K.K. Szabó, Phys. Lett. B **730**, 99 (2014).
- [6] T.M. Schwarz, S.P. Klevansky, and G. Papp, Phys. Rev. C **60**, 055205 (1999).
- [7] P. Zhuang, M. Huang, and Z. Yang, Phys. Rev. C **62**, 054901 (2000).
- [8] K. Fukushima, Phys. Rev. D **77**, 114028 (2008); K. Fukushima, Phys. Rev. D **78**, 039902 (E) (2008).
- [9] J.W. Chen, J. Deng, H. Kohyama, and L. Labun, Phys. Rev. D **93**, 034037 (2016).
- [10] H. Liu, J. Xu, L.W. Chen, K.J. Sun, Phys. Rev. D **94**, 065032 (2016).
- [11] H. Liu, Y.H. Yang, C. Yuan, M. Ju, X.H. Wu, and P.C. Chu, Phys. Rev. D **109**, 074037 (2024).
- [12] S.X. Qin, L. Chang, H. Chen, Y.X. Liu, and C.D. Roberts, Phys. Rev. Lett. **106**, 172301 (2011).
- [13] B.J. Schaefer and M. Wagner, Phys. Rev. D **85**, 034027 (2012).
- [14] W.J. Fu, Z. Zhang, and Y.X. Liu, Phys. Rev. D **77**, 014006 (2008).
- [15] W.J. Fu, J.M. Pawłowski, and F. Rennecke, Phys. Rev. D **101**, 054032 (2020).
- [16] M. M. Aggarwal et al., (STAR Collaboration), Phys. Rev. Lett. **105**, 022302 (2010).
- [17] L. Adamczyk et al., (STAR Collaboration), Phys. Rev. Lett. **112**, 032302 (2014).
- [18] J. Adam et al., (STAR Collaboration), Phys. Rev. Lett. **126**, 092301 (2021).
- [19] M. Abdallah et al., (STAR Collaboration), Phys. Rev. C **104**, 024902 (2021).
- [20] L. Adamczyk et al., (STAR Collaboration), Phys. Rev. C **92**, 014904 (2015).
- [21] J. Adam et al., (STAR Collaboration), Phys. Rev. C **103**, 034908 (2021).
- [22] L. Adamczyk et al., (STAR Collaboration), Phys. Rev. Lett. **112**, 162301 (2014).
- [23] L. Adamczyk et al., (STAR Collaboration), Phys. Rev. Lett. **120**, 062301 (2018).
- [24] M.I. Abdulhamid et al., (STAR Collaboration), Phys. Lett. B **845**, 138165 (2023).
- [25] M.I. Abdulhamid et al., (STAR Collaboration), Phys. Rev. Lett. **130**, 202301 (2023).
- [26] V.T. Cocconi, T. Fazzini, G. Fidecaro, M. Legros, N.H. Lipman, and A.W. Merrison, Phys. Rev. Lett. **5**, 19 (1960).
- [27] T.A. Armstrong, K.N. Barish, S. Batsouli, S.J. Bennett, M. Bertaina et al. (E864 Collaboration), Phys. Rev. C **61**, 064908 (2000).
- [28] W. Reisdorf et al. (FOPI Collaboration), Nucl. Phys. A **848**, 366 (2010).
- [29] J. Adam et al. (ALICE Collaboration), Phys. Rev. C **93**, 024917 (2016).
- [30] S. Acharya et al. (ALICE Collaboration), Phys. Rev. C **97**, 024615 (2018).
- [31] J. Chen, D. Keane, Y.G. Ma, A. Tang, and Z. Xu, Phys. Rep. **760**, 1 (2018).
- [32] J. Adam et al. (STAR Collaboration), Phys. Rev. C **99**, 064905 (2019).
- [33] L.P. Csernai and J.I. Kapusta, Phys. Rep. **131**, 223 (1986).
- [34] Y. Oh, Z. W. Lin, and C.M. Ko, Phys. Rev. C **80**, 064902 (2009).
- [35] K.J. Sun, L.W. Chen, C.M. Ko, J. Pu, and Z. Xu, Phys. Lett. B **781**, 499 (2018).
- [36] K.J. Sun, F. Li, and C.M. Ko, Phys. Lett. B **816**, 136258 (2021).
- [37] W. Zhao, C. Shen, C.M. Ko, Q. Liu, and H. Song, Phys. Rev. C **102**, 044912 (2020).
- [38] J. Steinheimer and J. Randrup, Phys. Rev. Lett. **109**, 212301 (2012).
- [39] C. Herold, M. Nahrgang, I. Mishustin, and M. Bleicher, Nucl. Phys. A **925**, 14 (2014).
- [40] F. Li and C. M. Ko, Phys. Rev. C **95**, 055203 (2017).
- [41] J. Steinheimer and J. Randrup, Phys. Rev. C **87**, 054903 (2013).
- [42] C. Herold, M. Nahrgang, I. Mishustin, and M. Bleicher, Phys. Rev. C **87**, 014907 (2013).
- [43] K.J. Sun, W.H. Zhou, L.W. Chen, C.M. Ko, F. Li, R. Wang, and J. Xu, arXiv:2205.11010.
- [44] Y. Nambu and G. Jona-Lasinio, Phys. Rev. **122**, 345 (1961).
- [45] Y. Nambu and G. Jona-Lasinio, Phys. Rev. **124**, 246 (1961).
- [46] M. Buballa, Phys. Rept. **407**, 205 (2005).
- [47] A. Bhattacharyya, S.K. Ghosh, S. Maity, S. Raha, R. Ray, K. Saha, S. Upadhaya, Phys. Rev. D **95**, 054005 (2017).

- [48] Z.B. Li, K. Xu, X.Y. Wang, M. Huang, *Eur. Phys. J. C* **79**,245 (2019).
- [49] K.J. Sun, C.M. Ko, S. Cao, and F. Li, *Phys. Rev. D* **103**, 014006 (2021).
- [50] Y.H. Yang, H. Liu, P.C. Chu, *Nucl. Sci. Tech.* **35**, 166 (2024).
- [51] K.J. Sun, L.W. Chen, C. M. Ko, and Z. Xu, *Phys. Lett. B* **774**, 103 (2017).
- [52] G. t'Hooft, *Phys. Rev. D* **14**, 3432 (1976); G. t'Hooft, *Phys. Rev. D* **18**, 2199 (E) (1978).
- [53] A. Bazavov et al. (HotQCD Collaboration), *Phys. Rev. D* **90**, 094503 (2014).
- [54] H.T. Ding, F. Karsch, and S. Mukherjee, *Int. J. Mod. Phys. E* **24**, 1530007 (2015).
- [55] L. Adamczyk et al., (STAR Collaboration), *Phys. Rev. C* **96** 044904 (2017).
- [56] B.I. Abelev et al., (STAR Collaboration), *Phys. Rev. C* **79**, 034909 (2009).
- [57] M. Motta, R. Stiele, W.M. Alberico, A. Beraudo, *Eur. Phys. J. C* **80**, 770 (2020).
- [58] W.M. Alberico, A. Beraudo, A. De Pace, A. Molinari, M. Monteno, M. Nardi, F. Prino, *Eur. Phys. J. C* **71**, 1666 (2011).
- [59] K.J. Sun, C.M. Ko, F. Li, J. Xu and L.W. Chen, *Eur. Phys. J. A* **57**,313 (2021)
- [60] W. Reisdorf et al. (FOPI Collaboration), *Nucl. Phys. A* **781**, 459 (2007).
- [61] S.S. Adler et al. (PHENIX Collaboration), *Phys. Rev. Lett.* **94**, 122302 (2005).
- [62] W. Zhao, K.J. Sun, C.M. Ko, and X. Luo, *Phys. Lett. B* **820**, 136571 (2021).